EDSU Journal of Engineering and Technology (EDSUJET) Vol. 2 (1), pp. 221 – 238. 2026
ISSN (Print):3121 – 8725 eISSN (Online): 3121 – 8597

Steady-state Thermal Loading and Performance Analysis of a Connecting Rod in a Diesel Engine

Stephen Olusegun Adediran[a]* and Festus Oamen Isaac[b]

[a]*Faculty of Engineering, Department of Mechanical Engineering, Edo State University Iyamho. Edo State, Nigeria.*
[b]*Faculty of Engineering, Department of Mechanical Engineering, Edo State University Iyamho. Edo State, Nigeria.*

*__Corresponding author__: stephenbelt2003@gmail.com

Received: 28th November 2025, Accepted: 07 February 2026, Published: 31 March 2026

K E Y W O R D S

ANSYS 2024 R1
AA356.0-T6;
Al7039/Cu/SiC;
Al7050-T7451;
Finite Element Method; Steady-state Analysis.

A B S T R A C T

This study investigated the suitability of three aluminum-based materials—AA356.0-T6, Al7039/Cu/SiC, and Al7050-T7451—for diesel-engine connecting rods through steady-state thermal analysis using the finite element method in ANSYS 2024 R1. The analysis assessed temperature distribution, heat flux, and derived thermal-resistance metrics to evaluate each material's thermal stability and susceptibility to fatigue under realistic operating conditions. All materials attained a comparable maximum temperature of approximately 1001 K, indicating similar thermal exposure. However, significant differences emerged in heat-transfer behaviour and deformation responses. Al7039/Cu/SiC exhibited the highest heat flux (8.669×10^5 W/m²), demonstrating superior heat conduction but lower thermal resistance, alongside the lowest thermal strain (0.01247 m/m). In contrast, AA356.0-T6 showed reduced heat flux but higher thermal expansion, resulting in greater thermo-mechanical strain (0.016 m/m). These results indicated that improved conductivity and lower expansion in Al7039/Cu/SiC effectively minimised temperature gradients and suppressed thermal strain. Overall, the finding concluded that Al7039/Cu/SiC offered the most favourable thermal performance and is therefore the preferred material for connecting-rod applications where efficient steady-state heat dissipation and dimensional stability were critical.

1.INTRODUCTION

Automotive sector is a very fast growing and developing sector which required cost reduction and quality improvement. Hence the need for constant innovations for optimum design in this sector is highly recommended. Research and Development projects and academic research are made frequently on this topic (Andreas, 2024). Engine is one of the basic components of

vehicles. Making innovations in engines, had influence on emission and performance of automobile directly. New designs for engine components are generally made to decrease weight, reduce cost and improve performances by providing desired conditions (Singh and Patel, 2021).

The connecting rod is a primary load-bearing component in reciprocating diesel engines, transmitting combustion forces from the piston to the crankshaft, experiencing complex combined mechanical and thermal loading throughout services. High peak combustion pressures, repeated cyclic loading and elevated operating temperatures create large thermal gradients and multi-axial stress states that govern both immediate structural performances and long-term fatigue life (Singh and Patel, 2021).
The finite element method (FEM) is a numerical technique for solving problems which are described by partial differential equations or can be formulated as functional minimization (Manohar & Karajagi, 2024). Finite element analysis (FEA) provides a robust framework to quantify steady-state thermal simulations. It identifies the temperature fields produced by combustion heat flux, convection, and mapped thermo-mechanical analyses. It predicts resulting stresses, deformations and fatigue indicators under realistic boundary conditions (Kumar, et al, 2021; Reddy, et al, 2021).

The study aims to design the connecting rod components using relevant analytical equations and developed a detailed 3D model of the connecting rod in SOLIDWORKS 2023. The model was subsequently imported into ANSYS 2024 R1, where steady-state thermal and structural analyses were performed. Through the steady-state thermal analysis, the temperature distribution and heat-flux patterns on the connecting rod were obtained. The analysis was performed on the following materials AA356.0-T6, Al7039/Cu/SiC, and Al7050-T7451 to evaluate deformations, thermal stresses, and overall performance, in order to identify the most suitable material for the connecting rod.

2. MATERIALS AND METHODS

The materials chosen for this study were AA356.0-T6, Al7050-T745 and Aluminum Metal Matrix Composites (MMC) Al7039/Cu/SiC. MMC was selected due its better thermal conductivity than aluminum alloys.

Tables 1 shows the Chemical composition of the connecting rod materials while Table 2 shows the Mechanical, Physical and Thermal properties of the selected materials for the connecting rod. Table 3 shows the specifications for WP10.33 diesel engine
H-Beam can take care of large stress and anxiety without flexing so used in high power engines. I -beam manages high-pressure, strong and lighter than corresponding H-Beam. In a study H-beam profile is better than I-beam profile because it has more stability – up to 43.1% and von Mises stresses are also less up to 12.3% (average – 15.7%). But I-beam is being used more as it is easier and less expensive to manufacture (Godara, Brenia, et al, 2022); hence I-beam is used for this study.

The Design Input parameters were obtained from the WP10.336 Weichai diesel engine.

Weichai Diesel Engine consists of six cylinders pistons. The details are as tabulated below (Weichai Power Company Limited, 2017), https://en.weichai.com/

Table 1: Chemical composition of the connecting rod materials

Element	AA 356.0-T6	Al7050-T7451	Al 7039/Cu/SiC
Iron, Fe (%)	0.6	0.15	0.35
Chromium,Cr (%)		0.04	0.1
Manganese,Mn (%)	0.35	0.1	0.03
Zinc, Zn (%)	0.35	5.7 – 6.7	0.05
Silicon, Si (%)	7.5	0.12	0.84
Silicon Carbide (%)			15
Al	90.1	87.3 – 90.3	69.22
Titanium, Ti	0.25	0.06	0.03
Zr		0.08 – 0.15	
Magnesium, Mg	0.45	1.9 – 2.6	0.02
Copper, Cu	0.25	2 – 2.6	12
Others	0.15	0.15	

(Source: ASM, 2019; Aerospace Metal, 2023; Teferi, 2025)

Table 2: Mechanical, Physical and Thermal properties of the connecting rod material

Element	AA 356.0-T6	Al7050-T7451	Al 7039/Cu/SiC
Tensile strength (MPa)	131MPa	524MPa	610MPA
Compressive Yield strength	90MPa	434MPa	400MPa
Shear modulus (typical for steel)	27.2GPa	26.9GPa	26.9GPa
Elastic modulus	72.4GPa	72GPa	100GPa
Poisson's ratio	0.33	0.33	0.30
Density(g/cm^3)	2.6	2.83	2.73
Thermal expansion co-efficient (µm/m°C)	21.4	23.6	18.55
Thermal conductivity (typical steel) (W/Mk)	150	157	169.6
Specific Heat(J/kg.K)	963	860	745.8

(Source: ASM, 2019; Aerospace Metal, 2023; Teferi, 2025)

2.1 Methodology

2.1.1 Overview

The methodology employed in this study followed a structured finite-element–based workflow consistent with established approaches in engine-component thermal analysis (Shigley et al., 2020; Reddy & Kothandaraman, 2019). The process comprised analytical design, 3D modelling, numerical simulation, extraction of thermal responses, and comparative material

evaluation.

2.1.2 Methods Applied

1. **Analytical Design of Connecting Rod Components**
   The connecting rod assembly—including piston pin, shank, big and small ends, crank-end cap, and cap bolts—was designed using standard mechanical design equations for axial loading, buckling, and fatigue, as recommended by Shigley's *Mechanical Engineering Design* (Shigley et al., 2020); Bhandari (2010) and Khurmi, and Gupta, (2005)

2. **3D Modelling in SOLIDWORKS 2023**
   The geometrically optimized design was modelled in SOLIDWORKS 2023, following modelling procedures for parametric solid components widely applied in engine-part research (Sharma & Pathak, 2018).

Table 3: Engine specifications for WP10.33 diesel engine

SN	Parameter	Symbol	Value	Unit
1	Engine Model	WP10.336		
2	Engine Type	Turbocharged-Intercool	6	Cylinders
3	Engine Capacity	V_s	9726	ml
4	Bore Diameter	d	126	mm
5	Stroke	s	130	mm
6	Con Rod Length	l	219	mm
7	Rated Speed	N	1900	rpm
11	Max Combustion Temperature		1001	K
12	Max Combustion Pressure	Pg	7.58	N/mm^2

3. **Importation into ANSYS Workbench**
   The SOLIDWORKS model was imported into ANSYS 2024 R1, consistent with workflows, described in comparative FEM studies of connecting rods (Liu et al., 2023; Rajasekaran & Reddy, 2021).

4. **Meshing of the Model**
   A uniform tetrahedral mesh size of **3 mm** was applied. Literature shows that mesh sizes between 2– 4 mm provide adequate convergence for connecting-rod thermal–structural analysis (Mokhtarishirazabad et al., 2013).

5. **Application of Boundary Conditions**
   Thermal loads, convection parameters, and mechanical constraints were applied to replicate peak operating conditions of diesel engines. Similar boundary-condition frameworks have been used in Farrahi & Azadi (2014) for rod and piston analyses.

6. **Steady-State Thermal and Performance Analysis**
   ANSYS steady-state thermal analysis was performed to compute **temperature**

distribution and **total heat flux**, aligning with standard heat-transfer evaluation methods (Incropera et al., 2017).

7. **Extraction of Temperature Gradient**
   Temperature gradients were obtained from nodal temperature fields, enabling assessment of thermo-mechanical stability—a method consistent with thermal-fatigue studies by Iswanto et al. (2018).

8. **Thermal Strain Calculation**
   Thermal strains were calculated for each material using
   $\epsilon_{th} = \alpha \Delta T$ (1)
   where α is the coefficient of thermal expansion. This approach is widely applied in material comparison studies under thermal stress (Callister & Rethwisch, 2021).

9. **Comparative Analysis and Material Selection**
   The thermal responses from AA356.0-T6, Al7039/Cu/SiC, and Al7050-T7451 were compared to determine the material exhibiting the most efficient heat dissipation and lowest thermal strain under steady-state conditions.

2.2 Assumptions

To enable computational feasibility, the following assumptions were adopted, consistent with assumptions in similar FEM studies (Mokhtarishirazabad et al., 2013; Liu et al., 2023):

i. Materials behave as **homogeneous**, **isotropic**, and **linearly elastic** under thermal loading.
ii. Convection coefficients remain constant during steady-state operation.
iii. Temperature-dependent material properties were approximated using average values within the operating temperature range.
iv. Bolt pretension effects and lubrication-film thermal resistance were neglected.
v. No plastic deformation occurs within the evaluated temperature field.

2.3 Limitations

The study is constrained by the following limitations:

i. Limited to the connecting rod for WP10.336 WEICHAI diesel engine specification which is presently used for 50 tons mobile crane in BUA Cement plc, OBU plant, Okpella, Etsako East, Edo state
ii. Only **steady-state** thermal behaviour was evaluated; transient thermal cycling was not included, which may influence fatigue life.
iii. Mechanical stresses from combustion pressure were not coupled with thermal loading in this phase of analysis.
iv. The FEM results depend on mesh density; although 3 mm provides convergence, finer meshes may refine localised gradients.
v. Real-world temperature fluctuations, lubrication effects, and dynamic inertia loads were simplified.

2.4 Boundary Conditions

Boundary conditions were defined based on typical diesel-engine environments as supported

by literature (Farrahi & Azadi, 2014; Incropera et al., 2017):

i. **Heat Source:** Uniform thermal load associated with peak combustion-temperature transfers through the piston pin into the small end.

ii. **Convection:** External convection applied to the rod surface using film coefficients corresponding to lubricated crankcase airflow.

iii. **Constraints:**

- Combustion pressure and heat were applied at the small end
- Big End is fixed.

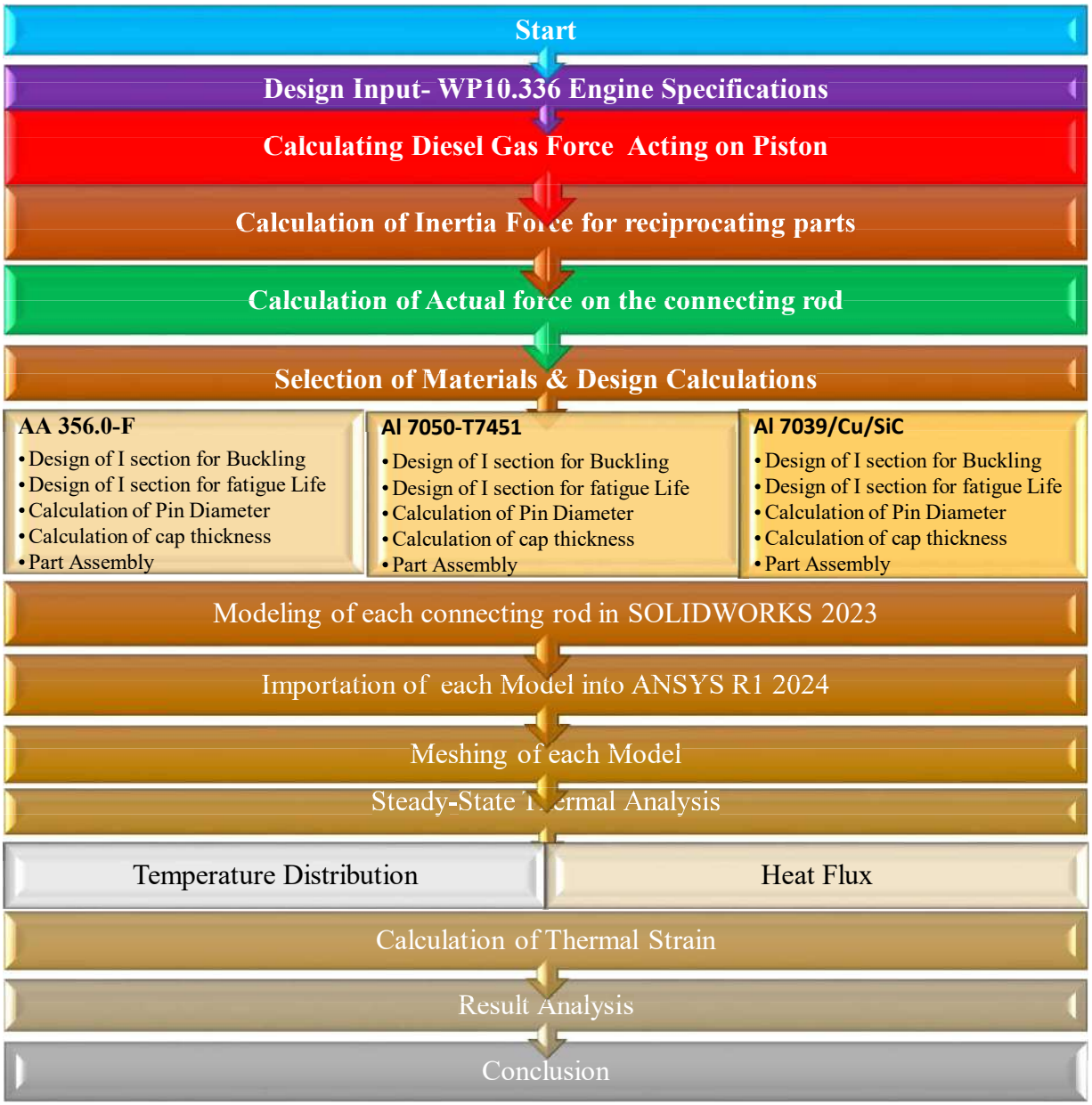

2.6 Design Calculations of Connecting Rods using the Selected Materials

2.6.1 Pressure for WEICHAI WP10.336 Diesel Engine

Max. speed = 1900rpm, Maximum combustion pressure =7.58MPa, Combustion Gas Temperature 1001K from weichai engine data.
All equations were obtained from Khurmi, R. and Gupta, J.K., (2005) A Textbook of Machine Design Text of Machine Design. Eurasia Publishing House (Pvt.) Ltd., New Delhi.]

2.6.2 Calculation of Force due Gas Pressure

$$F_p = P * A = P * \frac{\pi D^2}{4} \quad (2)$$

2.6.3 Calculation of force due to Inertia

$$Inertia\ Force, F_I = m \cdot \omega^2 \cdot r\left(cos\,\theta + \frac{cos\,2\theta}{n}\right) \quad (3)$$

$$n = \frac{l}{r} = \frac{2\times stroke}{stroke/_2} \quad (4)$$

Total Force acting $F = F_p \pm F_I$ (5)

Where,

F_P = force acting on the piston

F_I = force of inertia

$W_B = F \times F.S$, where F.S is safety factor and W_B = buckling force (6)

$$W_B = \frac{\sigma_c \cdot A}{1+a\left(\frac{L}{K_{xx}}\right)^2} \quad (7)$$

$A = 2(4t \times t) + 3t \times t = 11t^2$; where t is the thickness web thickness (8)

Moment of inertia of the section about X-axis: I_{xx}

$$I_{xx} = \frac{1}{12}[4t \times (5t)^3 - 3t(3t)^3] = \frac{419}{12}t^4 \quad (9)$$

Moment of inertia of the section about Y-axis: I_{yy}

$$I_{yy} = \left[2 \times \frac{1}{12}t \times (4t)^3 + \frac{1}{12}(3t)t^3\right] = \frac{131}{12}t^4 \quad (10)$$

2.6.4 Calculation of the radius of gyration

The radius of gyration about X- axis is

$$K_{xx} = \sqrt{\frac{I_{xx}}{A}} = \sqrt{\frac{419}{12}t^4 \times \frac{1}{11\,t^2}} = 1.7816t \quad (11)$$

2.6.5 Thermal Strain Calculation, ε_t

$$\varepsilon_t = \alpha\Delta T \quad (12)$$

3.0 RESULTS AND DISCUSSIONS

3.1 Calculation of Force due Gas Pressure

$F_p = 7.58 * \frac{\pi D^2}{4} = 7.58 * \frac{\pi(126)^2}{4} = 94527.1328N$ from equation (2)

3.1.1 Calculation of force due to Inertia

The maximum gas load occurs shortly after the dead centre position at θ = 3.3°, Cos3.3 = 0.9983≅ 1; from equations (2 and 3)

$$F_I = 1.394 \times \left(\frac{2\pi \times 1900}{60}\right)^2 \times 0.065 \times \left(1 + \frac{1}{4}\right) = 4483.8449$$

3.1.2 Total Force acting F ; from equation (5)

$$F = 94527.1328N - 4483.8449 = 90043.28794N$$

3.1.3 Buckling Load

Now let us find the dimensions of this I-section. Since the connecting rod is designed by taking the force on the connecting rod (F_P) equal to the maximum force on the piston (F_L) due to gas pressure, therefore, we know that the connecting rod is designed for buckling about X-axis (i.e. in the plane of motion of the connecting rod) assuming both ends hinged. Taking 2 as presumed safety factor, therefore the buckling load,

$W_B = F \times 2 = 180086.27588$ from equation (6)

3.1.4 Ratio of moment of inertia: equation (9) / equation (10)

$= \frac{I_{xx}}{I_{yy}} = 3.2$

Since the ratio of the moment of inertia of $I_{xx}\ to\ I_{yy}\ \ is\ 3.2\ the$ design shape satisfied the buckling condition.

3.2 Design Calculation for the Connecting Rod using AA 356.0-T6 Aluminum Alloy

$$\sigma_c = 90MPa;\ \ a = \frac{1}{9000};\ L = l = 219mm, ie\ connecting\ rod\ hinged\ at\ both\ ends$$
$$= 219mm\ from\ engine\ manual$$

3.2.1 Thickness of the I-section web, t;

from equations 5, 6, & 7

$$180086.27588 = \frac{90 \times 10^6 \times 11\ t^2}{1 + \frac{1}{9000} \times \left(\frac{0.219}{1.7816t}\right)^2} = \frac{99 \times 10^7\ t^4}{t^2 + 1.678902 \times 10^{-6}}$$

$$180086.27588\ (t^2 + 1.678902 \times 10^{-6}) = 99 \times 10^7 \times t^4$$

$$180086.27588\ t^2 + 0.3023477 = 99 \times 10^7\ t^4$$

$$-99 \times 10^7 t^4 + 180086.27588\ t^2 + 0.33244 = 0$$

$$t = -0.013417 \times 10^7 m;\ 0.013417 \times 10^7 m; (1.365696 \times 10^7 m)i; (-1.36569 \times 10^7 m)i$$

The solution gave two real roots and two complex roots, hence the selection of positive real root

$$\therefore t = 13.417mm \cong 13mm$$
$$H = 5t = 5 \times 13 = 65mm$$
$$B = 4t = 4 \times 13 = 52mm$$
$$H_1 = 1.25 * H = 1.25 * 65 = 81.25 \cong 81mm$$
$$H_2 = 0.9 * H = 0.9 * 65 = 58.5 \cong 59mm$$

The above calculations were applied to each of the materials and below are the designed dimensions

Table 4: Dimensions of designed connecting rod for the selected materials

Items Descriptions	Connecting rod Dimensions for selected Materials(mm)		
	AA 356.0-F	Al7050-T7451	Al 7039/Cu/SiC
Thickness of connecting rod (t)	13	6	7
Height of the section (H)	65	30	35
Width of the section (B)	52	24	28
Height at the Big End (H1)	81	38	44
Height at the small end (H2)	59	27	32
Inner diameter of the Small End(dp)	60	60	60
Outer diameter of the Small End(Dp)	86	86	86
Inner diameter of the Big End (dc)	88	88	88
Outer diameter of the Big End(Dc)	132	120	120
Thickness of the big end cap (t_c)	29	13	13

3.3 Steady-State Thermal Analysis using ANSYS 2024R1

3.3.1 AA365.0-T6 Steady-State Thermal Analysis

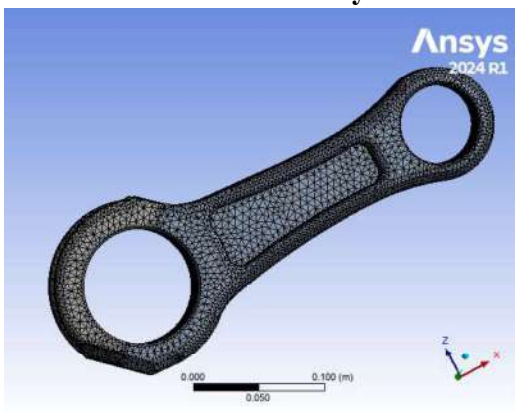

Figure 1 AA356.0-F Mesh

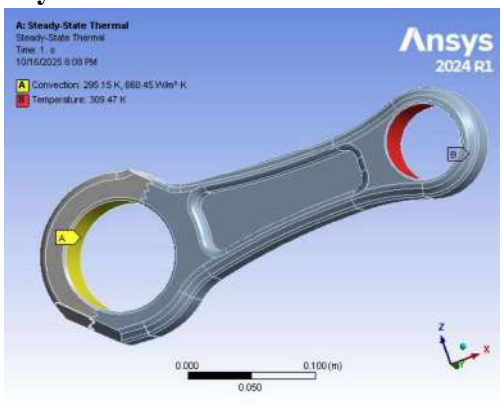

Figure 2 Boundary conditions

The steady-state thermal analysis of the AA356.0-T6 connecting rod was performed using ANSYS 2024 R1.

Figure 1 showed that the connecting rod was discretized using tetrahedral finite elements with a uniform element size of **3 mm**. The generated mesh consisted of **107,150 nodes** and **60,640 elements**, providing adequate resolution to capture temperature gradients in critical regions such as the big end, small end, and web section while maintaining computational efficiency.
Figures 2, 6 and 10 illustrate the steady-state thermal boundary conditions applied to the connecting rods AA356.0-T6, Al7039/Cu/SiC and Al7050-T7451 respectively. A convection

boundary with an ambient temperature of **295.15 K** and a heat transfer coefficient of **660.45 W/m²·K** was imposed on the external surfaces, while a fixed temperature of **1001 K** was applied at the small-end region to simulate heat input during engine operation.The purpose of this setup is to determine the temperature distribution within the connecting rod under realistic operating conditions.

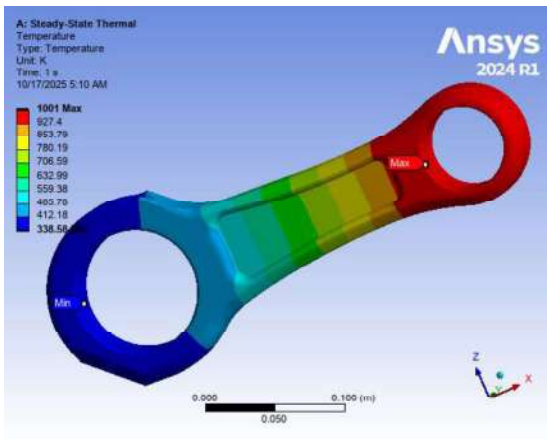

Figure 3: Temperature

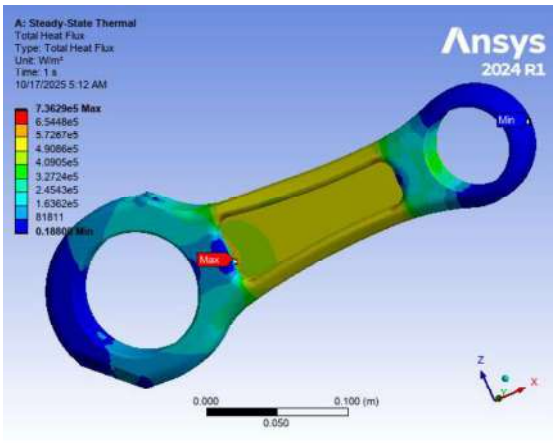

Figure 4: Heat Flux

Figure 3 shows the steady-state temperature distribution of the AA356.0-T6 connecting rod. The maximum temperature reaches **1001 K** at the small-end region, while the minimum temperature drops to **338.58 K** at the big end. This gradient confirms higher thermal loading near the piston-pin interface and effective heat dissipation along the rod.

The big end remains the coolest because it is connected to the crankshaft, which provides a larger heat sink and benefits from lubrication cooling.

Figure 4 presents the heat-flux contours for AA356.0-T6. The maximum heat flux is **7.329×10^5 W/m²**, occurring at the small-end transition zone, whereas the minimum heat flux is **0.18808 W/m²** at the big end. The distribution indicates efficient thermal conduction and limited risk of localized thermal-stress concentration.

3.3.2 Al7039/Cu/SiC Steady-State Thermal Analysis

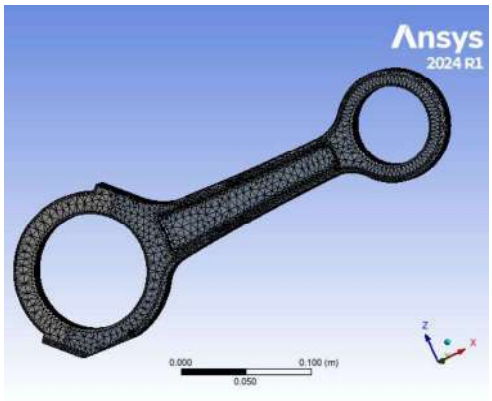

.

Figure 5: Al7039/Cu/SiC Mesh

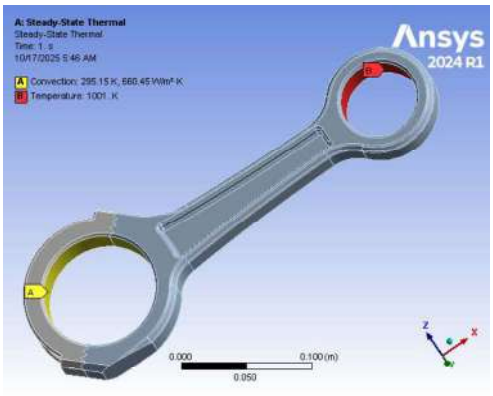

Figure 6: Boundary Condition

Figure 5 shows the finite element discretization of the Al7039/Cu/SiC connecting rod

developed in ANSYS 2024 R1. The geometry was meshed using tetrahedral solid elements with uniform size of 3 mm, resulting in approximately **80,297 nodes and 45,262 elements**, providing adequate refinement in critical regions such as the big-end, small-end, and shank to ensure accurate steady-state thermal predictions.

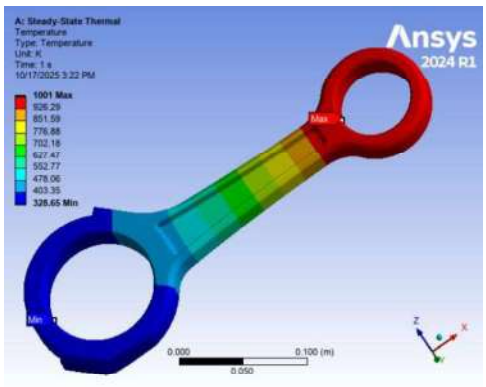

Figure 7: Temperature

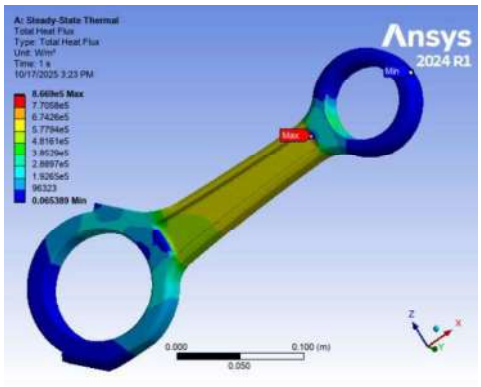

Figure 8: Heat Flux

Figure 7 presents the steady-state temperature distribution of the Al7039/Cu/SiC connecting rod obtained from ANSYS 2024 R1. The maximum temperature of approximately **1001 K** is observed at the small-end region, representing the heat input from the piston pin, while the minimum temperature of about **326.65 K** occurs near the big end due to heat dissipation. The smooth temperature gradient along the shank indicates effective heat conduction through the connecting rod under steady-state operating conditions.

Figure 8 illustrates the total heat-flux distribution in the Al7039/Cu/SiC connecting rod under steady-state conditions. The maximum heat flux is approximately **8.67×10^5 W/m²**, concentrated along the shank and fillet transition regions where temperature gradients are highest. The minimum heat flux of about **0.065 W/m²** is observed at regions exposed to convective cooling, indicating reduced thermal gradients and effective heat dissipation at the big-end region.

3.3.3 Al7050-T7451 Steady-State Thermal Analysis

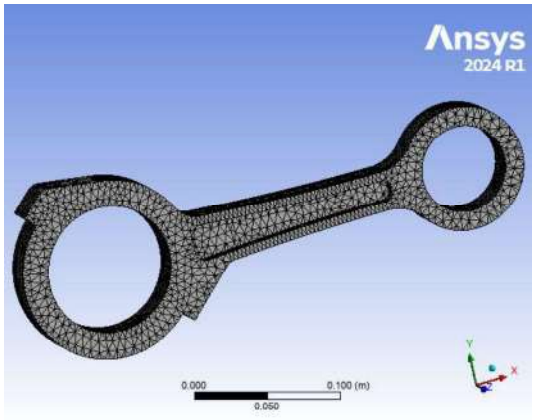

Figure 9: Al7050-T7451 Mesh

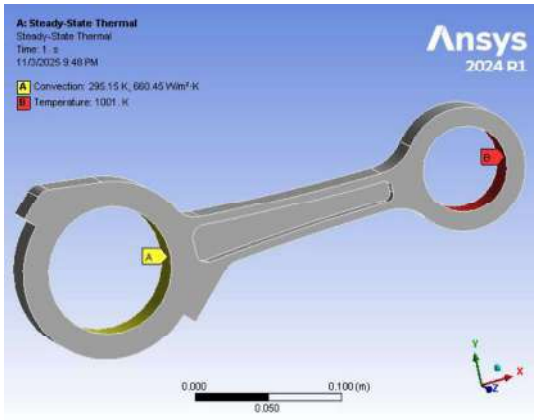

Figure 10: Boundary Condition

Figure 9 shows the finite element discretization of the Al7050-T7451 connecting rod developed in ANSYS 2024 R1. The geometry was meshed using tetrahedral solid elements with uniform size of 3 mm, resulting in approximately **39,617 nodes and 21,794 elements**, providing adequate refinement in critical regions such as the big-end, small-end, and shank to ensure accurate steady-state thermal predictions.

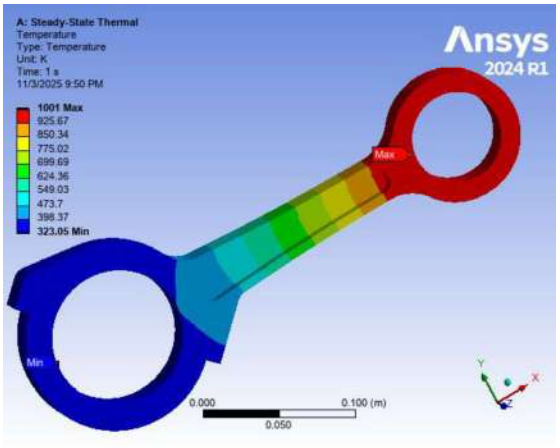

Figure 11: Temperature

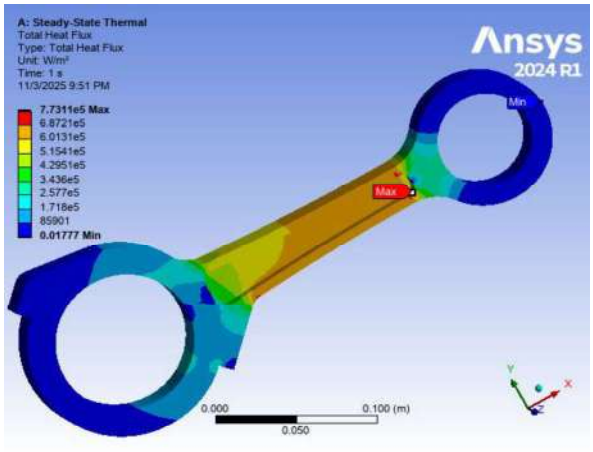

Figure 12: Heat Flux

3.3.4 Steady-State Thermal Analysis using ANSYS 2024R1 Simulation

The steady-state thermal analysis was conducted to evaluate heat distribution and thermal resistance among the candidate materials. All materials reached a similar maximum temperature of approximately 1001 K, indicating that they experience equivalent thermal exposure in service. However, differences were observed in the total heat flux, as illustrated in Figure 14, Al7039/Cu/SiC recorded the highest heat flux value, reflecting excellent heat conduction but lower thermal resistance. Conversely, AA356.0-T6 showed moderate heat flux, suggesting improved thermal stability and reduced risk of fatigue due to thermal cycling (Prasad and Wanhill, 2017).

Table 5 summarizes the steady-state thermal analysis result, detailing the maximum temperature and total heat flux for each material tested

Table 5: Result of Steady State Thermal Analysis

Model	Temperature(K)		Total Heat Flux (W/m^2)	
	Max	Min	Max	Min
AA356.0-T6	1001	339	7.36E+05	0.188
Al7039/Cu/SiC	1001	329	8.67E+5	0.0654
AlA7050-T7451	1001	323.05	7.7311E+5	0.01777

Table 5 summarizes the steady-state thermal response of the connecting rod for the three selected materials. While all materials experienced the same maximum applied temperature, variations in minimum temperature and total heat flux reflect differences in thermal conductivity and heat-transfer behavior, which influence their overall thermal performance.

Graphical Representation of Steady-State Thermal Analysis from Table 5

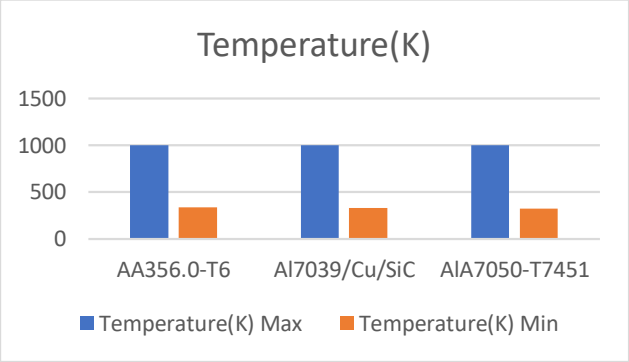

Figure 13 Temperature

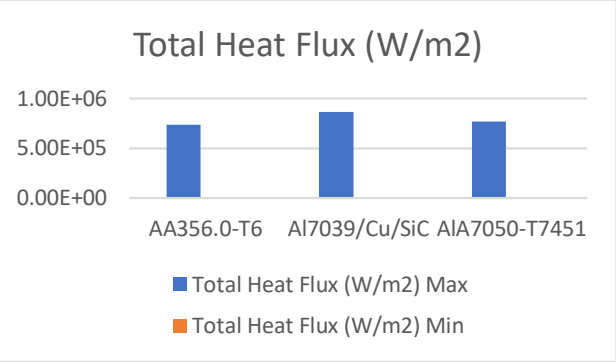

Figure 14 Total Heat Flux

Figure 13 compares the maximum and minimum temperatures of the connecting rod for the different materials, highlighting similar peak thermal exposure but noticeable differences in heat dissipation capability across the materials.
Figure 14 presents the maximum and minimum total heat flux values for the three materials, illustrating how material composition affects heat-transfer intensity and thermal gradient under steady-state operating conditions.

Table 6: Summary of Simulation Results

Model	Tmax (K)	Tmin (K)	ΔT = Tmax – Tmin (K)	q_{max} (W/m²)
AA356.0-T6	1001	339.0	662	7.36×10^5
Al7039/Cu/SiC	1001	329.0	672	8.67×10^5
AlA7050-T7451	1001	323.0	678	7.73×10^5

Thermal Strain Calculation, ε_t , from equation 12 and table 6

Table 7: Thermal Strain

Model	**ΔT(K)**	**α(µm/m°C)**	**$\varepsilon_t = \alpha\Delta T$ (m/m)**
AA356.0-T6	662	21.4	0.01417
Al7039/Cu/SiC	672	18.55	0.01247
AlA7050-T7451	678	23.6	0.016

3.3.5 Total Heat Flux (W/m²)

The material Al7039/Cu/SiC exhibited the lowest thermal resistance per unit area, indicating it is the most efficient in conducting heat under the imposed boundary conditions. The alloy AlA7050-T7451, although showing the lowest minimum temperature (Tmin = 323 K), has a slightly higher resistance owing to its moderate heat flux. Conversely, AA356.0-T6 shows the highest resistance and is therefore the least favourable thermally of the three.
The steady-state thermal simulations indicated that all three selected materials experienced the same imposed hot-spot temperature of 1001 K, but differ significantly in how heat is been

conducted away and in the resulting minimum temperature (Table 6). Such behaviour is consistent with earlier findings that material thermal conductivity and microstructural composition strongly influence heat dissipation patterns in aluminum alloys under high thermal loading (Kumar et al., 2021; Reddy et al., 2021). In the present results, Al7039/Cu/SiC exhibited the highest local total heat flux (8.67×10^5 W/m²), suggesting superior effective thermal conduction relative to AA356.0-T6 (7.36×10^5 W/m²) and Al7050-T7451 (7.73×10^5 W/m²) see Table 6 for detail. The corresponding temperature spans ($\Delta T \approx 662–678$ K) indicated very large thermal gradients across the connecting rod, consistent with the behaviour reported for high-performance aluminum engine components under similar loading (Rajasekaran et al., 2022; Singh & Patel, 2021). Using typical coefficients of thermal expansion for these alloys, the resulting thermal strains (Table 7) fall within ≈1.2–1.6%, large enough to generate substantial thermally induced stresses when geometric or mechanical constraints restrict free expansion. Overall, the higher conductivity and reduced effective thermal expansion of Al7039/Cu/SiC suppressed thermal strain (0.01247m/m) and improve thermal-fatigue resistance, whereas AA356.0-T6—with lower heat flux and higher thermal expansion exhibit greater susceptibility to thermo-mechanical distortion with thermal strain of 0.016m/m, see Table 7 for detail. Al7050-T7451, although intermediate in thermal behaviour, is expected to provide the highest mechanical safety margin due to its superior yield and fatigue strength, consistent with its performance in structural aerospace applications (Reddy et al., 2021).

4.0 Conclusion

Al7039/Cu/SiC with highest thermal conductivity value of 8.67×10^5 W/m² with lesser thermal stain of 0.01247m/m compared to other two materials were found to be of higher thermal-fatigue resistance

In practical terms, since the primary design objective is to maximise steady-state heat removal and minimise temperature gradients, Al7039/Cu/SiC is the preferred choice.

In conclusion, the study demonstrated that optimizing the connecting rod of the WP10.336 WEICHAI diesel engine with Al7039/Cu/SiC material enhanced its performances, efficiency, and reliability while reducing the likelihood of catastrophic failure caused by thermal stresses. The finding also provided valuable guidance for researchers and engineers in making informed decisions on material selection, design modifications, and operational conditions. These insights contribute to minimizing thermally induced failures and maximizing the overall efficiency, durability, and service life of diesel-engine connecting rods.

Theories Symbols

Symbols	Interpretation
σ_{t1}	maximum principal or normal stress in a bi-axial stress system
σ_{t2}	minimum principal stresses in a bi-axial stress system
σ_{yt}	Yield point stress in tension as determined from simple tension test
σ_u	Ultimate stress
τ_{max}	Maximum shear stress in a bi-axial stress system
τ_{yt}	Shear stress at yield point as determined from simple tension test

$\boldsymbol{\varepsilon_{max}}$	maximum principal (or normal) strain in a bi-axial stress system
$\boldsymbol{\varepsilon}$	Strain at yield point as determined from simple tension test
$\boldsymbol{l/m}$	Poisson's ratio
E	Young's modulus
F.S.	Factor of safety
$\boldsymbol{\sigma_C}$	Compressive yield stress
$\boldsymbol{W_B}$	Buckling load
$\boldsymbol{I_{xx}}$	Moment of inertia of the section about X-axis
$\boldsymbol{I_{yy}}$	Moment of inertia of the section about Y-axis
l	Length of the connecting rod
r	Radius of gyration
A	Cross-sectional area of the connecting rod
L	Equivalent length of the connecting rod
a	Rankine constant or =

Design Equations Parameters

Symbols	Interpretation
P_{max}	Maximum pressure of gas/effective pressure
D	Diameter of piston
A	Cross-section area of piston
$\boldsymbol{m_R}$	Mass of reciprocating parts (mass of piston, gudgeon pin, etc) $+\frac{1}{3}$rd mass of connecting rod
ω	Angular speed of crank
φ	Angle of inclination of the connecting rod with the line of stroke
θ	Angle of inclination of the crank from top dead centre
r	Radius of crank
$\boldsymbol{l}$	Length of connecting rod
n	Ratio of length of connecting rod to radius of crank = $\boldsymbol{l}$/r
n_c	Number of cylinders
S	Stroke length(m)
N	Speed of the Engine
L	Equivalent length of the connecting rod, Both ends Hinged L=l , Both ends fixed L = l/2
Z	Section modulus
$\boldsymbol{d_c}$	Diameter of the crank pin in mm
$\boldsymbol{l_c}$	Length of the crank pin in mm, = $1.25d_c$ to $1.5d_c$($1.25\boldsymbol{d_c}$)
$\boldsymbol{P_{bc}}$	Allowable bearing pressure in N/mm^2 = 7 to 12.5 N/mm^2 (9.8N/mm^2)
$\boldsymbol{d_p}$	Diameter of the piston pin in mm
$\boldsymbol{l_p}$	Length of the piston pin in mm, = $1.5d_p$ to $2d_p$($\boldsymbol{1.75d_p}$)
$\boldsymbol{P_{bp}}$	Allowable bearing pressure for piston pin bush in N/mm^2 = 10.5 to 15 N/mm^2(15N/m^2)
$\boldsymbol{d_{cb}}$	Core diameter of the bolt in mm

σ_t	Allowable tensile stress for the material of the bolts in MPa
n_b	Number of bolts. Generally, two bolts are used
d_b	Major Diameter of the Bolt
t_c	Thickness of the big end cap
σ_b	Bending stress
R	Number of rings
P_R	Pressure of rings (0.025 to 0.04 N/mm2)
μ	Coefficient of friction (about 0.1).
b_c	Width of the cap in mm. It is equal to the length of the crankpin or big end bearing (*lc*)

Abbreviations

FEM	Finite Element Method
FEA	Finite Element Analysis
IC	Internal Combustion
ICEs	Internal Combustion Engines
F.S.	Factor of Safety
UTM	Universal Test Machine
RPM	Revolution per Minute
MMCs	Metal matrix composites

ACKNOWLEDGEMENTS

First and foremost, I give all glory, honour, and adoration to the Almighty God, the source of wisdom, knowledge, and strength, for His endless grace and divine guidance throughout my academic journey. His favour and mercy have been my firm foundation, granting me perseverance and clarity to complete this dissertation successfully. Without His divine support, none of this would have been possible.

I sincerely appreciate the Dean of the Faculty of Engineering, Engr. Prof. John Wasiu, for his exemplary leadership, academic excellence, and commitment to quality education. My profound gratitude also goes to the Head of the Department of Mechanical Engineering, Engr. Dr. S. Nihad Achekuogene, for his continuous support, motivation, and encouragement. I am deeply indebted to my Supervisor, Engr. Dr. F. Oamen Isaac, whose valuable guidance, patience, and constructive criticisms greatly shaped this research work. My appreciation equally extends to the academic and technical staff of the Department of Mechanical Engineering for their assistance, as well as my colleagues and classmates for their cooperation, friendship, and shared academic experiences.

Finally, I express my heartfelt gratitude to my beloved wife Mrs. B. Elizabeth Adediran, and lovely children in the family for their unconditional love, prayers, and moral support throughout this academic pursuit. Special thanks to my friends most especially late Pastor A. Ebenezer Ajayi, mentors, my bosses and colleagues at work for their understanding,

encouragement, and inspiration during this journey. Their constant belief in my abilities and unwavering support has been instrumental in the successful completion of this dissertation.

REFERENCES

Andreas Ochsner, (2024) Collaborative research advancing engineering solutions for real-world challenges, pages 54-64.

ANSYS (2023). ANSYS Topology Optimization User's Guide. ANSYS, Inc

Bhandari, V. B. (2010). Design of machine elements. Tata McGraw-Hill.

Callister, W. D., & Rethwisch, D. G. (2021). Materials science and engineering. Wiley.

Farrahi, G. H., & Azadi, M. (2014). Thermal–mechanical analysis of engine components. Applied Thermal Engineering.

Godara,S.S., Brenia,V., Soni A. K., Shekhawat R. S., and Saxena K.K.,(2022), Design and analysis of connecting rod using ANSYS software, Materialstoday Proceedings, Volume 56, Part 4, April 2022, Pages 1896-1903, https://doi.org/10.1016/j.matpr.2021.11.166

Incropera, F. P., DeWitt, D. P., Bergman, T. L., & Lavine, A. S. (2017). Fundamentals of heat and mass transfer. Wiley.

Iswanto, P. et al. (2018). Thermal fatigue evaluation of aluminium alloys.

Khurmi, R. and Gupta, J.K., (2005) A Textbook of Machine Design Text of Machine Design. Eurasia Publishing House (Pvt.) Ltd., New Delhi.]

Kumar S.,VermaV., Gupta N,(2021) Design and FEM Analysis of Connecting Rod of different Materials, Lecture note in Mechanical Engineering, Springer Singapore

Liu, Y. et al. (2023). FEM-based thermal analysis of connecting rods.

Lunn, K. F. (2024). Thermal and Electrical Conductivity of Aluminum Alloys: A Critical Review. Materials and Design, 225, 111–[pages].

Manohar G., Prof. Prashant K., (2024), Optimization and Analysis of 4-Wheeler Connecting Rod for Weight Reduction and Performance Enhancement

Mokhtarishirazabad, M. et al. (2013). Thermo-mechanical behaviour of reciprocating engine parts.

Orhadahwe, T. A. (2020). A Review on Primary Synthesis and Secondary Treatment of Aluminium-Matrix Composites. Advances in Engineering Materials, 22(3), 1-20.

Rajasekaran, K. S. K., & Reddy, V. (2021). FEM analysis of connecting rods under thermal load.

Rajasekaran, M., et al. (2022). Thermo-mechanical behaviour of aluminum alloys under cyclic engine loading. International Journal of Mechanical Engineering Research.

Reddy, K. S. K., Kannan, M., & Karthikeyan, R. (2021). Evaluation of Mechanical and Thermal Properties of Aluminium-7475 Reinforced with Graphite and Fly Ash. E3S Web of Conferences, 85, 01186. https://doi.org/10.1051/e3sconf/20218501186

Reddy, K. S. K., Prasanth, T. M., & Rao, V. V. (2021). Thermal and structural analysis of aluminum alloys for high-temperature engine applications. Journal of Materials Engineering and Performance.

Sharma, R., & Pathak, M. (2018). CAD–FEM analysis of connecting rods.

Shigley, J. E., et al. (2020). Mechanical engineering design. McGraw-Hill.

Singh, A., & Patel, R. (2021). Finite element assessment of lightweight connecting rods for improved fuel efficiency in diesel engines. Journal of Mechanical and Industrial Engineering Research, 9(2), 45–53.

Singh, R., & Patel, K. (2021). Finite-element-based assessment of thermal gradients and stress development in light-alloy engine components. Materials Today: Proceedings

Teferi, F. T., Kolhe K. P., Tsegaw A. A., & Fatoba S. O. (2025) Optimization of SiC reinforced Al7039/Cu composites for enhanced thermal conductivity and hardness via response surface methodology, Published 8 January 2025, IOP Publishing Ltd, Materials Research Express, Volume 12, Number 1, https://doi.org/10.1088/2053-1591/ada2e3

Weichai Power Company Limited (2017), Operation and Maintenance Manual for WP10 Series Four-valve Diesel Engine (China IV, V), June 2017